Supporting Information

Anomalous Adsorption Behavior of CO_2 in Aqueous Hydrazine

Byeongno Lee,[a] Haley M. Stowe,[b] Kyu Hyung Lee,[a] Nam Hwi Hur,[a,†] Son-Jong Hwang,[c,†] Eunsu Paek,[b] Gyeong S. Hwang[b,†]

[a] Department of Chemistry, Sogang University, Seoul 04107, Korea

[b] Department of Chemical Engineering, University of Texas at Austin, Austin, Texas 78712, United States

[c] Division of Chemistry and Chemical Engineering, California Institute of Technology, Pasadena, California, 91125, United States

[†] e-mail: sonjong@cheme.caltech.edu, nhhur@sogang.ac.kr, gshwang@che.utexas.edu

I.　　General Information

I-1. Materials

Hydrazine hydrate (**HH**, 64%wt solution) ($NH_2NH_2 \cdot H_2O$, 98%), ^{15}N labeled hydrazine hydrate ($^{15}NH_2{}^{15}NH_2 \cdot H_2O$, 98%), and ^{13}C labeled carbon dioxide ($^{13}CO_2$, 99 atom % ^{13}C, <3 atom % ^{18}O) were purchased from Sigma-Aldrich. All reagents were used without any further purification. The **HH** was further diluted with de-ionized water to prepare sorbents in different concentrations. The 1:1 adduct of hydrazine and carbon dioxide is a zwitterionic solid ($^+NH_3NHCO_2^-$, **4-s**), denoted as hydrazine carboxylate (**HC**), and was prepared by a method described in the literature[1]. **Precaution:** The **HC**, **4-s**, is very stable in a closed bottle. However, it could be harmful for health due to its sublimation character when it is exposed to air. At ambient conditions, the vapor pressure of hydrazine in 24wt % aqueous solution is expected to be about 5,000 ppm. Accordingly, effective ventilation equipment is highly recommended for handling both the solid **HC** and **HH** solution to avoid vapor inhalation. See the MSDS and the related reports for details.[2]

I-2. Experimental setup
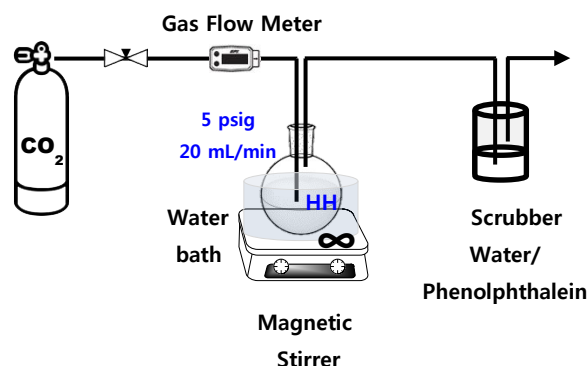
Figure S1 Setup for the preparation of the CO_2-hydrazine reaction products.

II.   Supplemental Experimental NMR data

II-1. Experimental NMR results for formation of zwitterionic solid $^+NH_3NHCOO^-$ (4-s) from $[^+NH_3NH\text{-}COO^-]$ + NH_2NH_2 (2-b)

^{13}C NMR spectrum shown in Figure S2-a was obtained after 30 min of CO_2 bubbling into **HH**. The weight gain showed that the CO_2 loading (χ) was 64 mol%. CO_2 capture by hydrazine and subsequent formation of carbamate species appears to increase the viscosity of the product solution. Foaming caused by gas bubbling was easily visible and it filled up the vessel as the bubbling time approaches to 30 min. In another words, it was difficult to perform uniform gas bubbling at such high level of CO_2 loading. As described in the main text (I-3), two ^{13}C resonances at 165.5 and 164.5 ppm represent the formation of di-carbamate and mon-carbamates, respectively. The equilibrium in the mono-carbamates, i.e. **2-a** $\leftrightarrow$ **2-b** (see Scheme I) is shifted to populate more **2-b** in the solution, represented by the significant upfield shift of ^{13}C resonance of mono-carbamates. The concentration ratio between di- and mono-carbamates, K'(=[di-carbamate]/[mono-carbamate]), was 5.8. An interesting observation was the downfield shift (164.5 to 166.0 ppm) of ^{13}C resonance of mono-carbamates as shown in Figure S2-b when a ^{13}C NMR spectrum was retaken from the exact same NMR sample after a few days in the laboratory at room temperature. During this storage period, no weight change was detected. The total ^{13}C signal intensities for two spectra (Figure S2-a and b) was reduced by ~ 10% and the K' was reduced to 3.8. First, the signal loss without mass change can be attributed to part of signal that became invisible in the NMR experimental setup. Note that ^{13}C NMR in this case is optimized for detection of carbonaceous species in the solution phase. Carbon species in the solid state can be invisible. Second, the downfield shift and the decrease of K' indicate that the χ value is lowered in the solution phase. We can only speculate that such change is possible either by adding free hydrazine to the solution or by some physical change that release free hydrazine to the system. We later discovered that there was precipitation of mono-carbamate **2-b** to form **4-s** (see Scheme I), which explained the ^{13}C NMR signal loss. The precipitation resulted in freeing hydrazine molecules in solution phase and became available for the **2-a** $\leftrightarrow$ **2-b** equilibrium shift, explaining the chemical shift change. Furthermore, the experimental results suggest that precipitation is energetically favored as the **2-b** species becomes more probable relative to **2-a** (upfield shift in ^{13}C NMR), and aggregation, followed by cluster formation, and eventual solidification occurs. As a matter of fact, it is possible to directly prove the presence of

$H_3N^+NHCOO^-$ (**4-s**) in solid state, as demonstrated below by taking advantage of the solid NMR setup.
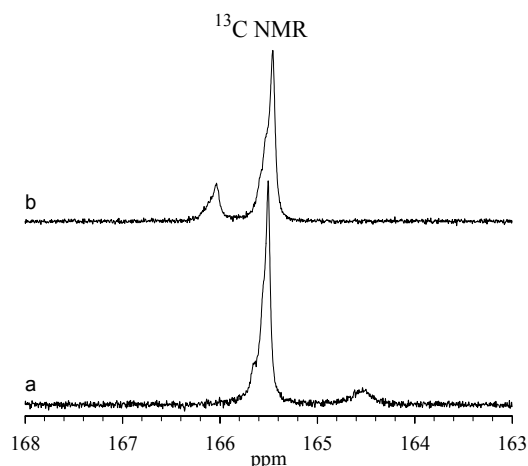
Figure S2 ^{13}C NMR (200 MHz Bruker DSX spectrometer) spectra of a product solution: a) right after 30 min bubbling of CO_2 to **HH** (64 wt% hydrazine), b) the same sample after a few days at room temperature. No weight change was detected for both NMR samples. Sample was spun at 1.5 kHz.

A separate CO_2 capture experiment was performed, similarly using the CO_2-**HH** (**1**) sorbet, while in this case extended CO_2 bubbling period (t>30 min) was applied. ^{13}C NMR spectrum taken immediately after reaction is shown in Figure S3-a. The spectrum looks unique in showing nearly a single resonance at 165.4 ppm, an indication of di-carbamate formation. However, we believe mono-carbamates were also present and their resonance position happened to be overlapped with the di-carbamate because of the up-field shift. The shoulder of the peak in fact suggests the presence of mono-carbamates. When the sample was stored in the lab overnight, we observed the emergence of 166.4 ppm resonance, an indication of the recovery of mono-carbamate in the solution phase. The result is consistent with the observation described in Figure S2.
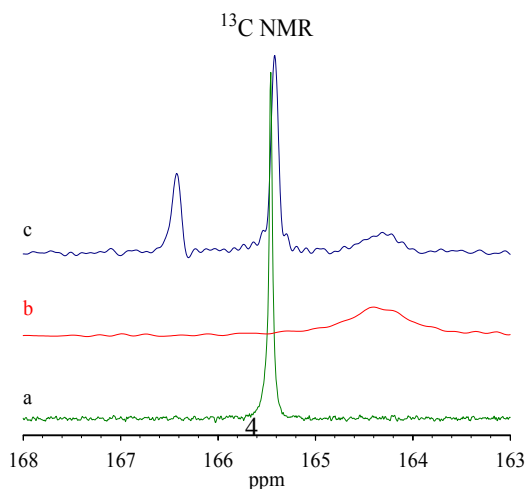
Figure S3 a) ^{13}C MAS NMR (DSX-500 MHz) of liquid aliquot taken from a reaction of **HH**+CO_2 bubbling reaction at 15 °C for extended period (t>30 min). b) ^{13}C CPMAS NMR (1 ms contact time and 8 kHz spinning), c) ^{13}C MAS NMR spectrum obtained using longer recycle delay time (d1=4000 s).

However, there was noticeable ^{13}C signal loss although no loss in sample amount was noted. At higher spinning rate (12 kHz), we detected a broad resonance with spinning sidebands underneath of sharp peak in ^{1}H MAS NMR spectra. The observation led us to conclude the carbamates solidified during the storage period. Another broad resonance at 164.3 ppm became visible only after the recycle delay time was drastically increased (d1=4000 s) as shown in Figure S3-c. We attributed the peak to the solid phase $H_3N^+NHCOO^-$ (**4-s**) as its position was matched precisely with that of solid sample $H_3N^+NHCOO^-$ (see next section). Furthermore, it was possible to observe same resonance using cross-polarization (CP) MAS NMR method[3] as shown in Figure S3-b. Note that the other two carbon resonances (mono- and di-carbamates) were absent in CPMAS NMR because they are present in liquid phase.

II-2. Solid state ^{13}C CPMAS NMR characterization of hydrazine carboxylate (HC), 4-s.

Zwitterionic solid, **4-s**, $^+NH_3-NH-COO^-$, is colorless crystalline solid, which was isolated from the hydrazine and pressurized CO_2 reaction.[1,4] Its crystal structure and solid state NMR characterizations are available in the literature[1] showing zwitterionic arrangement of the molecule. When ^{13}C MAS NMR (see Figure S4) was further analyzed using similarly prepared solid powder, the spinning sidebands due to characteristic shielding anisotropy of the carbonyl carbon were effective to yield its shielding parameters: δ_{iso}=164.3, CSA=61.2 ppm, η=0.71. The **HC** is known to be insoluble in most of organic or inorganic solvents while its sublimation property can be further utilized in some solvent-less organic syntheses.[5,6]

5
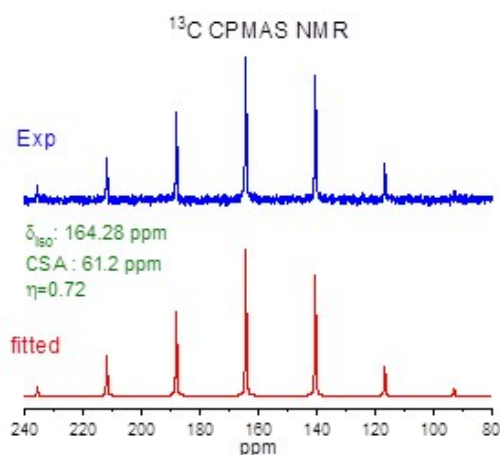
Figure S4 Solid state ^{13}C CPMAS NMR spectrum (11.7 T) and a fitted spectrum of the solid compound **4-s**. Fit parameters are as listed in the plot and δ_{iso} and η are isotropic chemical shift and asymmetry parameter of chemical shift anisotropy (CSA), respectively. The sample was spun at 3 kHz and during CPMAS experiment which employed a 0.5 ms of contact pulse with rf pulse power of 63 kHz. ^1H spin-lattice relaxation time was about 15 sec while ^{13}C spins was found to relax much slowly ($T_1\sim$ 300 s) at 11.7 T and at ambient condition.

## II-3. Equilibrium between mono- and di-carbamates in water
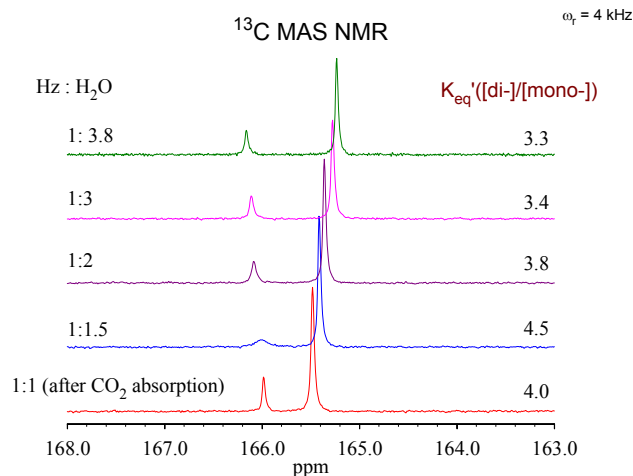
Figure S5 ^{13}C MAS NMR spectra as a function of water content in solution of mono- and di-carbamates that were reaction products from which hydrazine hydrate (NH_2-NH_2·H_2O) was bubbled with CO_2 gas at 15 °C.

During a CO_2 capture experiment using hydrazine sorbent, product solution was extracted at a certain time point so that the two species, mono- (**2-a** and **2-b**) and di-carbamates (**3**), are unequally populated.

6

Figure S5 shows that variation of water content did not shift the equilibrium noticeably although there is minor decrease in the equilibrium constant K'_{eq} (=[di-carbamate]/[mono-carbamate]), showing slightly favorable environment for mono-carbamates when heavily diluted by water. Note as well that mono- and di-carbamates show the opposite direction in progressive movement of their positions, indicating deshielding and shielding effect for mono- and di-carbamates, respectively, as more water molecules are involved in the hydrogen bonding networks. Understanding of the difference requires taking account all contributions of hydrogen bonding to the carbonyl carbons in two molecules, and it is out the scope of this work.

II-4.   Chemical exchange rate between mono- and di-carbamates via ^{13}C EXSY NMR
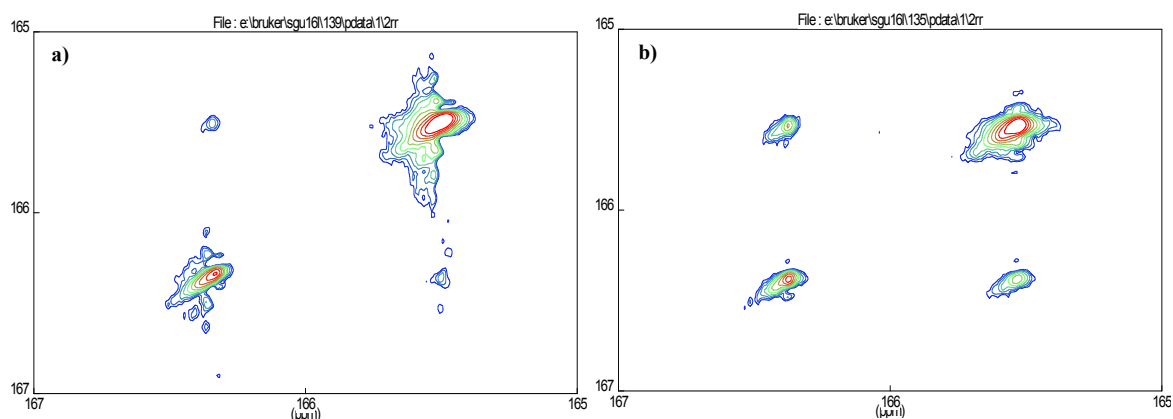
Figure S6 Two dimensional (2D) ^{13}C EXSY spectrum of hydrazine-CO_2 reaction, after 20 min of CO_2 bubbling (see Fig. 1-d). a) mixing time =0.1 s, b) mixing time = 0.5 s.

Exchange spectroscopy (EXSY) is a two dimensional (2D) NMR pulse sequence for measuring exchange reaction rates, and it is particularly suitable for quantifying dynamic processes in the range of tens of milliseconds to several seconds.[7,8] In the sequence, there is a mixing period where chemical exchange reactions are allowed to take place during so-called the mixing time, t_m, resulting in redistribution of the nuclear magnetizations among exchanging resonances. In this way, the exchanging sites are identified via observation of cross peaks in a 2D NMR spectrum, and the cross peak intensity at a certain t_m can be used to extract the dynamics parameters. For example, chemical exchange between two carbamate species, mono- (**2-a↔2-b**, 166.5 ppm) and di-carbamates (**3**, 165.6 ppm), leads to generation of cross peaks as shown in Figure S6. The cross peaks become stronger as the mixing time

was increased from 0.1 s to 0.5 s (see 2D contour plots in Fig. 6-a and b, respectively), indicating that the reaction rate is slow and within the proper range for the technique. In a given mixing time, t_m, the exchange rate constant, k_{ex}, can be calculated from a matrix that is composed of normalized peak intensities of diagonal and cross peaks of 2D EXSY spectrum.[8] Exchange rates were obtained from two different samples and they are summarized in Table S1. The rate constant was raised by about 10 times as the CO_2 loading (χ) was increased slightly more (61.2 to 64 mol%). At this environment, all molecules may be in hydrogen bonding network and arranged to create an environment that allows fast H^+ transfer, N-C bond break up, CO_2 release, and CO_2 pick up by un-protonated hydrazine (NH_2NH_2) reactions. In other words, CO_2 may be said "loosely coupled" by the capturing agent. In this state, CO_2 from carbamates can be released without high energy penalty. Note that CO_2 release from carbamates needs energies in the order of 40-60 kcal/mole[9].

Table S1. Exchange rate constant measured for mono- and di-carbamate via 2D EXSY NMR spectroscopy

Reaction time (min) and χ (mol%)	K'(=[di-]/[mono-carbamate])	^{13}C T_1 (s)	Rate constant, k (s^{-1})
20, χ=61.2	2.9	1.3	1.2
30, χ=64	5.8	1.3	13.4

II-5. ^{13}C variable temperature (VT) NMR for probing exchange reaction between carbamates (mono- and di-carbamates).

The chemical transformation between two carbamates molecules (**2-a↔2b** and **3**), see Scheme I) were further investigated using ^{13}C variable temperature (VT) MAS NMR. The experimental data are presented in Fig. 7 in the main text, and provided here are simulated spectra at various temperatures with change in the exchange correlation time (τ_c) constant as a function of temperature. A two site exchange model[10] was employed for fitting VT NMR spectra using Origin® V8.0 software. (see Fig. S7).

13C VT MAS NMR

110 °C
100 °C
90 °C
85 °C
80 °C
70 °C
50 °C
RT

168   167   166   165   164
ppm
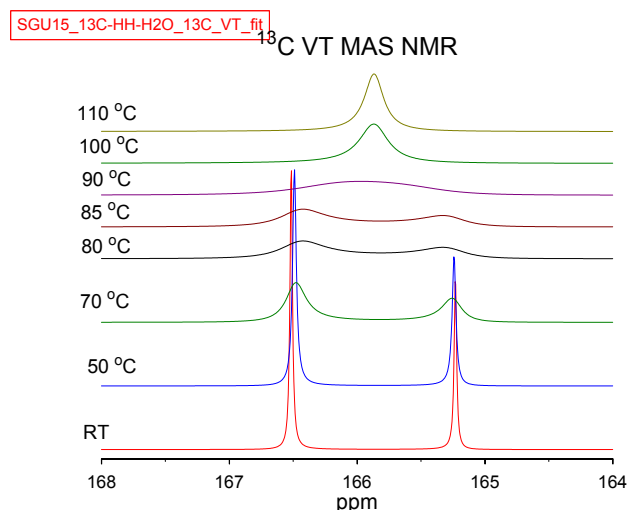
Figure S7 ^{13}C VT MAS NMR fitted for spectra shown in Fig. 8 in the main text. ^{13}C VT MAS spectra were recorded at temperatures shown in the plot while about 100 micro-litter of solution sample was heated in *in situ* in a NMR sample rotor with leak free and high temperature Vespel cap. Sample was spun at 4 kHz. ^{13}C NMR signal before and after VT experiment confirmed no change in intensities of mono- and di-carbamates.

III.   Supplemental Theoretical Studies

III-1.   AIMD (*Ab initio* molecular dynamics) simulations of CO_2 reaction with aqueous hydrazine

In the simulations, 6 NH_2NHCOO^-, 6 $N^+H_3NH_2$, 6 CO_2, and 12 H_2O molecules were placed in a cubic box of edge length 11.73 Å with periodic boundary conditions, corresponding to our experimental condition of HH reacting with CO_2 while, here, multiple CO_2 molecules were intentionally inserted to increase the probability of the CO_2 + NH_2NH_2 reaction, but did not affect the elementary events we present. The simulations were carried out in the NVT ensemble at 400 K.   These simulations clearly demonstrate (1) hydrazine reaction with CO_2 forming mono-carbamate via the two-step zwitterion mechanism, i.e., NH_2NH_2 + CO_2 → $NH_2NH_2^+COO^-$ + NH_2NH_2 → $^+NH_3NH_2 \cdot NH_2NHCOO^-$ [**2-a**] and (2) fast H$^+$ transfer between mono-carbamate and free hydrazine, i.e., $NH_2NHCOO^- \cdot {}^+NH_3NH_2$ (**2-a**) ↔ $^+NH_3$-NH-COO$^- \cdot NH_2NH_2$ (**2-b**).

III-2.   AIMD simulations of conversion of HCO_3^- to NH_2NH-COO^-

9
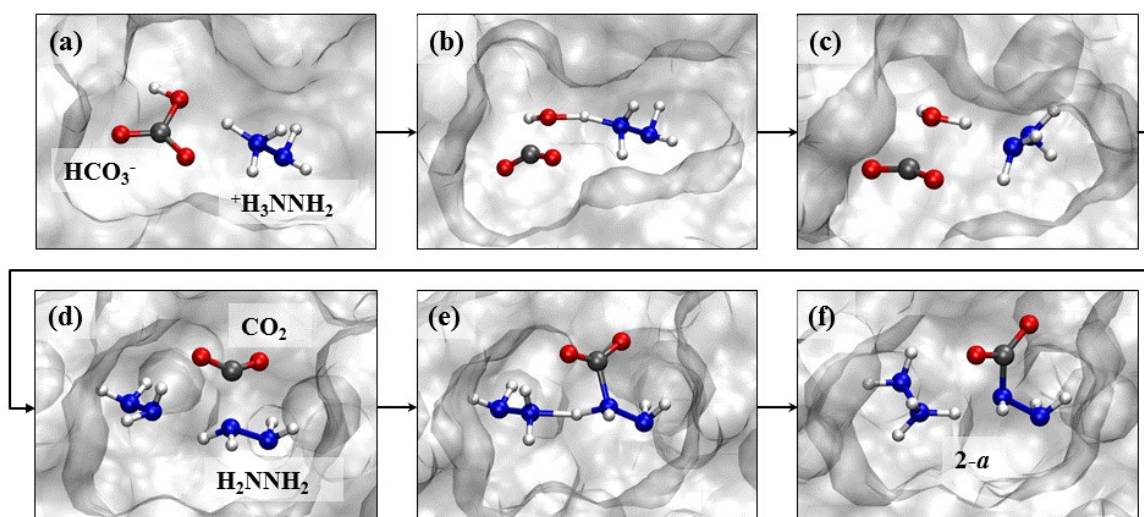
Figure S8 AIMD snapshots demonstrating CO_2 release from HCO_3^- when proton (in $H_3^+NNH_2$) is available nearby, i.e. $HCO_3^- + {}^+NH_3NH_2 \rightarrow H_2O + CO_2 + N_2H_4$ [(a) $\rightarrow$ (c)]. The released CO_2 then reacts with N_2H_4 to form $NH_2NH\text{-}COO^-$ and ${}^+NH_3NH_2$ via the zwitterion intermediate [(d) $\rightarrow$ (e) $\rightarrow$ (f)]. The system contains 1 HCO_3^-, 1 ${}^+NH_3NH_2$, 5 N_2H_4, and 17 H_2O molecules in a cubic periodic box of edge length 9.52 Å, corresponding to approximately 30 wt% hydrazine solution.

In the simulations, 1 HCO_3^-, 1 ${}^+NH_3NH_2$, 5 NH_2NH_2, and 17 H_2O molecules were placed in a cubic periodic box of edge length 9.52 Å, corresponding to approximately 30 wt% hydrazine solution. As shown in Figure S8, HCO_3^- can be easily converted to H_2O and CO_2 if a proton is available nearby, i.e., $HCO_3^- + {}^+NH_3NH_2 \rightarrow H_2O + CO_2 + NH_2NH_2$ [(a) $\rightarrow$ (c)]. The released CO_2 can then react with NH_2NH_2 to form the zwitterion intermediate [(d) $\rightarrow$ (e)], which will deprotonate to a nearby NH_2NH_2 to form $NH_2NH\text{-}COO^-$ and ${}^+NH_3NH_2$ [(e) $\rightarrow$ (f)]. Here, the AIMD simulations were carried out at 1,000 K; the high temperature was used in order to speed up the reaction so as to identify probable elementary events within the limited simulation time span. Note that although the concentration of hydrazine used in the AIMD simulations is somewhat lower than the 10:1 [NH_2NH_2]:[HCO_3^-] ratio used in the experimental work, we expect that conversion to mono-carbamate would be even more likely to occur in the latter case due to the larger availability of hydrazine. Note that bicarbonate formation in aqueous solution is known to have a higher reaction barrier than carbamate formation from the CO_2 reaction with amines.[11]

III-3. Quantum Mechanical (QM) calculations of NMR chemical shifts

We used the Gaussian 09 suite of programs[12] for the QM calculations at the B3LYP/6-311++G(d,p) level of theory. Figure S9 shows the cluster models and the predicted ^{13}C NMR chemical shifts. The SMD model of Truhlar and co-workers[13] within the polarizable continuum approach was employed to model the solvent implicitly. The Gauge-Independent Atomic Orbital method[14] was used to estimate nuclear shielding, which were converted to chemical shifts using $\delta = \sigma_{TMS} - \sigma$ where σ_{TMS} is the predicted isotropic shielding constant of tetramethylsilane (TMS).
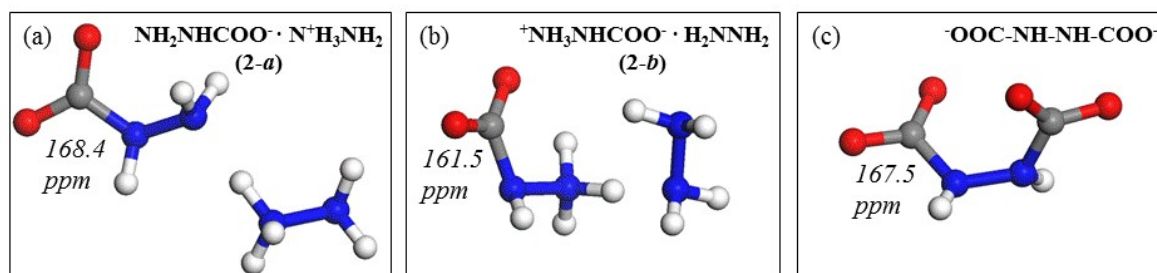
Figure S9. Predicted ^{13}C NMR chemical shifts in ppm for the model clusters mimicking (a) un-protonated mono-carbamate, (b) protonated mono-carbamate, and (c) di-carbamate from static QM calculations at the B3LYP/6-311++G(d,p) level of theory using the GIAO method and SMD solvation model.

As shown in Figure S9, our calculations predict that the ^{13}C shift of di-carbamate [(c)] is upfield about 1 ppm from un-protonated mono-carbamate **2-a** [(a)], which supports our assignment of the peak appearing at $\chi \sim 30$ in the ^{13}C spectra to di-carbamate formation.   In addition, the ^{13}C shift of protonated mono-carbamate [(b)] **2-b** is predicted to be significantly upfield from **2-a**.   Since **2-a** and **2-b** are indistinguishable on the ^{13}C NMR spectra due to fast H^+ exchange, yielding only a single ^{13}C resonance, we attribute the upfield shift of the peak representing the average of their contributions with increasing χ to the increasing formation of **2-b** relative to **2-a**.

III-4.   AIMD-predicted thermodynamic favorability

The Helmholtz free energy changes ($\Delta A = \Delta E - T\Delta S$) of selected reactions were estimated by calculating ΔE and ΔS from AIMD simulations at 298 K.   The two-phase thermodynamics (2PT) method[15–17] was employed to calculate the absolute entropy of each aqueous amine system considered.   This method has already been proven quite successful in predicting the entropy of a liquid system from a relatively short MD trajectory (10-20 ps)

after equilibrium is reached. [15–18]   Here, the entropies were estimated from a trajectory of 30 ps in the NVT ensemble at 298 K where the trajectory files were recorded every 1 fs.   In order to enhance sampling of the small systems from AIMD simulations, we averaged the energies from at least 5 cases with different initial configurations.   We have shown that the entropy values tend to converge after 20 ps in aqueous amine systems.[19]

In addition to predicting entropy changes from molecular motion ($S_M = S_{translational} + S_{rotational} + S_{vibrational}$) of each aqueous amine system, we also considered the change in configurational entropy due to the composition difference between the reactant and product systems.   The configurational entropy in cal/mol CO_2/K is given by $S_C = -Nk\sum x_i ln x_i$ where N is the number of hydrazine per CO_2, k is the Boltzmann constant, and x_i is the fraction of NH_2-NH_2/$^+NH_3NH_2$/NH_2NHCOO^-/$^+NH_3$-NH-COO^-/^-OOC-NH-NH-COO^- relative to the total amount of NH_2-NH_2.

Table S2.   Predicted changes in the total energy (ΔE in kcal/mol CO_2), entropy (ΔS in cal/mol CO_2/K), and Helmholtz free energy (ΔA in kcal/mol CO_2) from AIMD simulations at 298 K for the $2NH_2NH$-COO^- + $2^+NH_3NH_2$ → ^-OOC-NH-NH-COO^- + 2^+NH_3-NH_2 + NH_2NH_2 reaction in **HH** at varying CO_2 loadings ($\chi = CO_2$ mol % with respect to NH_2NH_2). The corresponding numbers of amine species in the reactant (S_R) and product (S_P) sides placed in a cubic periodic box with edge length (as specified in Å) are also listed.   Systems also contain 12 H_2O molecules, corresponding to **HH**.

χ	ΔE	ΔS $= (\Delta S_M + \Delta S_C)$	ΔA	Composition		Edge Length
				S_R	S_P	
17	0.76	9.75 = (11.49 − 1.74)	-2.15	8 NH_2-NH_2, 2 $^+NH_3NH_2$, 2 NH_2NHCOO^-	9 NH_2-NH_2, 2 $^+NH_3NH_2$, 1 ^-OOC-NH-NH-COO^-	10.41
33	0.60	2.09 = (2.61 − 0.52)	-0.03	4 NH_2-NH_2, 4 $^+NH_3NH_2$, 4 NH_2NHCOO^-	6 NH_2-NH_2, 4 $^+NH_3NH_2$, 2 ^-OOC-NH-NH-COO^-	10.15
50	0.63	-1.19 = (-2.57 + 1.38)	-0.36	6 $^+NH_3NH_2$, 6 NH_2NHCOO^-	3 NH_2-NH_2, 6 $^+NH_3NH_2$, 3 ^-OOC-NH-NH-COO^-	10.51

Table S2 displays the calculated free energy change (ΔA) for the 2 NH_2NH-COO^- + 2 $^+NH_3NH_2$ → ^-OOC-NH-NH-COO^- + 2 $^+NH_3$-NH_2 + NH_2NH_2 reaction at varying CO_2

loadings (χ = CO_2 mol % with respect to NH_2NH_2) in monohydrate hydrazine from AIMD simulations.   The corresponding numbers of amine species in the reactant (S_R) and product (S_P) sides placed in a cubic periodic box with edge length (as specified in Å) are also listed; 12 H_2O molecules are also included in each S_R and S_P.

Table S3. Total entropies (cal/mol/K) used in ΔE, ΔS, and ΔA calculations from AIMD simulations at 298 K.   Each system contains 30 H_2O and 1 N_2H_4, $NH_2NH\text{-}COO^-$, or HCO_3^- molecules in a cubic periodic box with side length as indicated.   Note that for H_2O there are 30 H_2O molecules total.

	N_2H_4	$NH_2NH\text{-}COO^-$	HCO_3^-	H_2O
S	410.7	417.6	383.4	354.6
Box Size (Å)	9.84	9.90	10.01	9.65

We also used this approach to evaluate the thermodynamic favorability of the HCO_3^- + $N_2H_4 \rightarrow NH_2NH\text{-}COO^- + H_2O$ reaction.   Here, each molecule was placed in a cubic periodic box with 30 H_2O molecules.   Note that this calculation assumes that the hydrazine species are fully dispersed and well-hydrated in approximately 6 wt% hydrazine solution.   The predicted absolute entropies are displayed in Table S3 below; the change in configurational entropy (ΔS_C) will be 0. ΔE, ΔS, and ΔA are predicted to be 11.7 kcal/mol CO_2, -10 cal/mol CO_2, and 14.7 kcal/mol CO_2, respectively for the HCO_3^- + $N_2H_4 \rightarrow NH_2NH\text{-}COO^- + H_2O$ reaction.

IV.   References

1   B. Lee, S. H. Kang, D. Kang, K. H. Lee, J. Cho, W. Nam, O. H. Han and N. H. Hur, *Chem. Commun.*, 2011, **47**, 11219–21.

2   J. K. Niemeier and D. P. Kjell, *Org. Process Res. Dev.*, 2013, **17**, 1580–1590.

3   J. Schaefer and E. O. Stejskal, *J. Am. Chem. Soc.*, 1976, **98**, 1031–1032.

4   K. H. Lee, B. Lee, J. H. Lee, J. K. You, K. T. Park, I. H. Baek and N. H. Hur, *Int. J. Greenh. Gas Control*, 2014, **29**, 256–262.

5   B. Lee, P. Kang, K. H. Lee, J. Cho, W. Nam, W. K. Lee and N. H. Hur, *Tetrahedron Lett.*, 2013, **54**, 1384–1388.

6   B. Lee, K. H. Lee, B. W. Lim, J. Cho, W. Nam and N. H. Hur, *Adv. Synth. Catal.*, 2013, **355**, 389–394.

7   S. Macura and R. R. Ernst, *Mol. Phys.*, 1980, **41**, 95–117.

8   C. L. Perrin and T. J. Dwyer, *Chem. Rev.*, 1990, **90**, 935–967.

9   W. Andreoni and F. Pietrucci, *J. Phys. Condens. Matter*, 2016, **28**, 503003.

10   V. Římal, H. Štěpánková and J. Štěpánek, *Concepts Magn. Reson. Part A*, 2011, **38A**, 117–127.

11   S. Gangarapu, A. T. M. Marcelis, Y. a. Alhamed and H. Zuilhof, *ChemPhysChem*, 2015, **16**, 3000–3006.

12   M. J. Frisch, G. W. Trucks, H. B. Schlegel, G. E. Scuseria, M. A. Robb, J. R. Cheeseman, G. Scalmani, V. Barone, B. Mennucci, G. A. Petersson, H. Nakatsuji, M. Caricato, X. Li, H. P. Hratchian, A. F. Izmaylov, J. Bloino, G. Zheng, J. L. Sonnenberg, M. Hada, M. Ehara, K. Toyota, R. Fukuda, J. Hasegawa, M. Ishida, T. Nakajima, Y. Honda, O. Kitao, H. Nakai, T. Vreven, J. A. Montgomery, J. E. Peralta, F. Ogliaro, M. Bearpark, J. J. Heyd, E. Brothers, K. N. Kudin, V. N. Staroverov, T. Keith, R. Kobayashi, J. Normald, K. Raghavachari, A. Rendell, J. C. Burant, S. S. Iyengar, J. Tomasi, M. Cossi, N. Rega, J. M. Millam, M. Klene, J. E. Knox, J. B. Cross, V. Bakken, C. Adamo, J. Jaramillo, R. Gomperts, R. E. Stratmann, O. Yazyev, A. J. Austin, R. Cammi, C. Pomelli, J. W. Ochterski, R. L. Martin, K. Morokuma, V. G. Zakrzewski, G. A. Voth, P. Salvador, J. J. Dannenberg, S. Dapprich, A. D. Daniels, O. Farkas, J. B. Foresman, J. V. Ortiz, J. Cioslowski and D. J. Fox, *Gaussian09 Revis. C.01*, Gaussian, Inc., Wallingord CT, 2010.

13   A. V Marenich, C. J. Cramer and D. G. Truhlar, *J. Phys. Chem. B*, 2009, **113**, 6378–6396.

14   K. Wolinski, J. F. Hinton and P. Pulay, *J. Am. Chem. Soc.*, 1990, **112**, 8251.

15   S.-T. Lin, M. Blanco and W. A. Goddard, *J. Chem. Phys.*, 2003, **119**, 11792.

16   S.-T. Lin, P. K. Maiti and W. A. Goddard, *J. Phys. Chem. B*, 2010, **114**, 8191–8198.

17   T. A. Pascal, S.-T. Lin and W. A. Goddard, *Phys. Chem. Chem. Phys.*, 2011, **13**, 169–81.

18   T. A. Pascal, D. Schärf, Y. Jung and T. D. Kühne, *J. Chem. Phys.*, 2012, **137**, 244507.

19   H. Stowe, E. Paek and G. S. Hwang, *Phys. Chem. Chem. Phys.*, 2016, **18**, 25296–25307.